Spitzer Space Telescope spectroscopy of ices toward low-mass embedded protostars

Boogert, A.C.A.; Pontoppidan, K.M.; Lahuis, F.; Dishoeck, E.F. van

Version:	Not Applicable (or Unknown)
License:	Leiden University Non-exclusive license
Downloaded from:	https://hdl.handle.net/1887/2209

Note: To cite this publication please use the final published version (if applicable).

SPITZER SPACE TELESCOPE SPECTROSCOPY OF ICES TOWARD LOW-MASS EMBEDDED PROTOSTARS[1,2]

A. C. Adwin Boogert,[3] Klaus M. Pontoppidan,[4] Fred Lahuis,[4,5] Jes K. Jørgensen,[4] Jean-Charles Augereau,[4] Geoffrey A. Blake,[6]
Timothy Y. Brooke,[3] Joanna Brown,[3] C. P. Dullemond,[7] Neal J. Evans, II,[8] Vincent Geers,[4] Michiel R. Hogerheijde,[4]
Jacqueline Kessler-Silacci,[8] Claudia Knez,[8] Pat Morris,[9] Alberto Noriega-Crespo,[9] Fredrik L. Schöier,[4]
Ewine F. van Dishoeck,[4] Lori E. Allen,[10] Paul M. Harvey,[8] David W. Koerner,[11] Lee G. Mundy,[12]
Philip C. Myers,[10] Deborah L. Padgett,[9] Anneila I. Sargent,[3] and Karl R. Stapelfeldt[13]

ABSTRACT

Sensitive 5–38 μm *Spitzer Space Telescope* and ground-based 3–5 μm spectra of the embedded low-mass protostars B5 IRS1 and HH 46 IRS show deep ice absorption bands superposed on steeply rising mid-infrared continua. The ices likely originate in the circumstellar envelopes. The CO_2 bending mode at 15 μm is a particularly powerful tracer of the ice composition and processing history. Toward these protostars, this band shows little evidence for thermal processing at temperatures above 50 K. Signatures of lower temperature processing are present in the CO and OCN^- bands, however. The observed CO_2 profile indicates an intimate mixture with H_2O, but not necessarily with CH_3OH, in contrast to some high-mass protostars. This is consistent with the low CH_3OH abundance derived from the ground-based *L*-band spectra. The $CO_2 : H_2O$ column density ratios are high in both B5 IRS1 and HH 46 IRS ($\sim$35%). Clearly, the *Spitzer* spectra are essential for studying ice evolution in low-mass protostellar environments and for eventually determining the relation between interstellar and solar system ices.

Subject headings: astrochemistry — infrared: ISM — ISM: abundances — ISM: molecules — stars: formation — stars: individual (B5 IRS 1)

1. INTRODUCTION

A recurring question in disk, planet, and comet formation studies is how the composition of molecular material evolves as it flows from the molecular cloud to the protostellar envelope and protoplanetary disk. Much of the material in these environments is frozen on grains. A plethora of processes, including heating by stellar photons, shocks related to accretion or outflow, cosmic-ray hits, and ultraviolet irradiation, can change the ice structure and composition. The spectroscopic effects of these processes can be observed in the vibrational bands of the ices through infrared spectroscopy. Ices around high-mass protostars have been extensively studied in this way. *Infrared Space Observatory* (*ISO*) spectra have shown that in particular the ice structure is affected by heating from the central star. The simplicity of the ice composition does indicate that the formation of new species through ultraviolet irradiation or cosmic-ray hits occurs at a low level at best. Observations of ices around low-mass protostars have been limited because of the unavailability of much of the 5–20 μm spectral region, where many of the molecular bending-mode transitions occur. In particular, the CO_2 bending mode at 15 μm is a valuable tracer of ice structure and composition (Ehrenfreund et al. 1998; Gerakines et al. 1999). With the sensitive Infrared Spectrometer (IRS; Houck et al. 2004) on board the *Spitzer Space Telescope*; Werner et al. 2004), this band can now be observed for the first time at high quality in low-mass systems.

Observations of two protostars are presented in this paper. B5 IRS 1 (IRAS 03445+3242; Beichman et al. 1984; $L = 10\ L_\odot$) is well studied at infrared and millimeter wavelengths (e.g., Charnley et al. 1990; Langer et al. 1996). The millimeter continuum emission is resolved on a few arcsecond scale, and it may originate in an inclined disk. The outflow has received most of the attention, and it has a large opening angle, leading to significant outflow/infall interaction. HH 46 IRS (IRAS 08242−5050; $L = 12\ L_\odot$) is also deeply embedded and is also the driving source of a powerful outflow. *Spitzer* imaging and spectroscopic observations of this source, focused on the outflow, are presented in Noriega-Crespo et al. (2004).

2. OBSERVATIONS

B5 IRS 1 and HH 46 IRS were observed with *Spitzer* IRS as part of the "c2d" *Spitzer* Legacy program (Evans et al. 2003) in the modules Short-Low (SL; $\lambda = 5$–14 μm; $R = 64$–128), Short-High (SH; $\lambda = 10$–20 μm; $R = 600$), and Long-High (LH; $\lambda = 20$–38 μm; $R = 600$). The archival *Spitzer* AOR keys

[3] Division of PMA, MC 105-24, California Institute of Technology, Pasadena, CA 91125.

[4] Leiden Observatory, P.O. Box 9513, 2300 RA Leiden, Netherlands.

[5] SRON, P.O. Box 800, 9700 AV Groningen, Netherlands.

[6] Division of GPS, MC 150-21, California Institute of Technology, Pasadena, CA 91125.

[7] Max-Planck-Institut für Astrophysik, P.O. Box 1317, D-85741 Garching, Germany.

[8] Department of Astronomy, University of Texas at Austin, 1 University Station C1400, Austin, TX 78712-0259.

[9] *Spitzer* Science Center, California Institute of Technology, Pasadena, CA 91125.

[10] Smithsonian Astrophysical Observatory, 60 Garden Street, MS 42, Cambridge, MA 02138.

[11] Department of Physics and Astronomy, Northern Arizona University, Box 6010, Flagstaff, AZ 86011-6010.

[12] Department of Astronomy, University of Maryland, College Park, MD 20742.

[13] Jet Propulsion Laboratory, California Institute of Technology, MC 183-900, 4800 Oak Grove Drive, Pasadena, CA 91109.
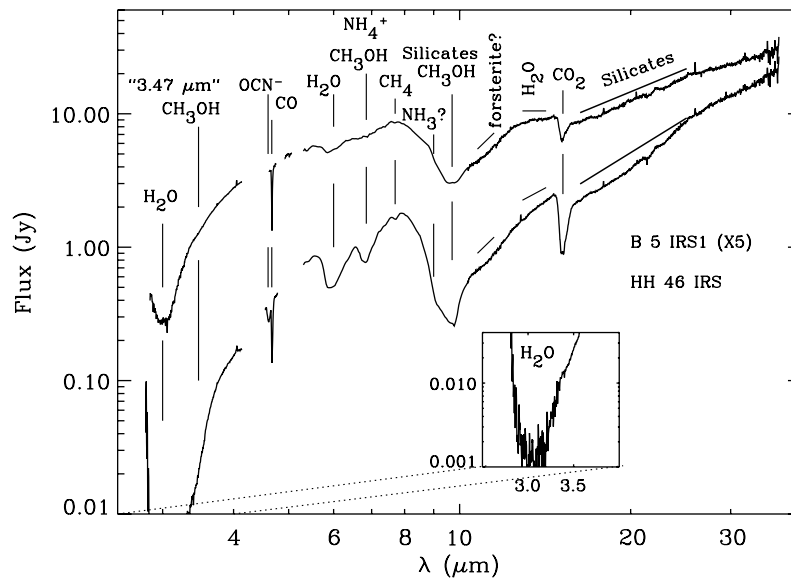
FIG. 1.—Combined *Spitzer* and ground-based *L*- and *M*-band spectroscopy of B5 IRS 1 (*top*; multiplied by factor of 5 for clarity) and HH 46 IRS (*bottom*). Identifications and possible identifications are indicated.

are 0005638912 (HH 46 IRS) and 0005635328 (B5 IRS 1) for Program ID (PID) 172. Both sources are well centered in all slits. The integration time was 28 s per module per source at 14 s ramps, except for SH, which has 24 s in total and 6 s ramps. The spectra were reduced with the IRS pipeline version 9.5 on 2004 March 10 at the *Spitzer* Science Center. Bad pixels were interpolated in the spectral domain in the two-dimensional images before extracting one-dimensional spectra. Accurate wavelength calibration was assured using calibration tables available in 2004 May. For overlapping SH spectral orders, the poorly calibrated long-wavelength part of each order was removed. This is particularly important for obtaining a reliable profile of the CO_2 ice band at 15.2 μm, where two orders overlap. HH 46 IRS was observed independently as an Early Release Observation (PID 1063, AOR key 0007130112; Noriega-Crespo et al. 2004). The data sets are in good agreement and were averaged. Finally, complementary ground-based observations were obtained. B5 IRS 1 was observed with Keck NIRSPEC (McLean et al. 1998) at $R = 25,000$ in the *M* band and at $R = 2000$ in the *L* band. Very Large Telescope ISAAC (Moorwood et al. 1999) *L*- and *M*-band spectra of HH 46 IRS were obtained at $R = 600$ and 5000, respectively. The *Spitzer* and ground-based spectra were combined by scaling the ground-based data.

3. RESULTS

The combined *Spitzer* and ground-based 3–38 μm spectra of B5 IRS 1 and HH 46 IRS show steeply rising continua (Fig. 1). The continuum of HH 46 IRS is the steepest, with a 35/4 μm flux ratio of 100, compared to 10 for B5 IRS 1. Numerous silicate and ice absorption features are superposed. The main ice constituents are H_2O, CO_2, and CO. The well-known, yet unidentified, 3.47 and 6.85 μm bands are present in both sources as well. Rarely seen before is a shallow absorption feature at 11.2 μm in both sources. It may be related to refractory dust components, such as crystalline forsterite (Kessler-Silacci et al. 2004). In addition, HH 46 IRS, but not B5 IRS 1, shows absorption by CH_4 and "XCN" (likely OCN^-; van Broekhuizen et al. 2004). Finally, other ice features may be present in the 5–10 μm region (NH_3, HCOOH), but a dedicated analysis is

required to verify their reality. We focus on the band profiles and abundances of the main ice components and their relation to the 15 μm CO_2 bands, discovered with *Spitzer*.

The CO_2 bending mode has rarely been observed toward low-mass protostars, and never at such high quality. It is blended with the short-wavelength wing of the silicate bending mode. The CO_2 band is put on an optical depth scale, assuming that the "intrinsic" profile of the silicate band is represented by the Galactic center source GC 3 (Chiar et al. 2000). For this a third-order polynomial is fitted to the wavelength regions 13.0–14.7 and 26.3–33.3 μm. The resulting CO_2 bands look similar to those observed in other lines of sight (Fig. 2*b*); note in particular the presence of a long-wavelength wing extending to at least 16 μm (Gerakines et al. 1999). Similar to the massive protostar NGC 7538 IRS 9 weak double ice crystallization peaks are observed at the bottom of the band in HH 46 IRS, but not in B5 IRS 1. Neither B5 IRS 1 nor HH 46 IRS show evidence for a third peak at 15.38 μm, expected in $CH_3OH : CO_2$ complex formation.

To place the interpretation of the CO_2 band within a larger perspective, ground-based observations of the 3.53 μm CH_3OH band and the 4.67 μm band of solid CO are analyzed. The 3.53 μm band is superposed on the wing of the strong 3.07 μm H_2O band and is locally blended with the unidentified 3.47 μm band. Following Brooke et al. (1999), we derive the continuum and separate the CH_3OH contribution. For comparison, spectra of the massive protostars W33A (Brooke et al. 1999) and NGC 7538 IRS 9 (Boogert et al. 2004) are analyzed as well. Hints of CH_3OH are seen in both HH 46 IRS and B5 IRS 1 (Fig. 2*a*), resulting in column densities of 7% with respect to H_2O, comparable to NGC 7538 IRS 9, but much less than W33A. For HH 46 IRS the detection of CH_3OH is strengthened by the presence of a feature at 9.7 μm in the bottom of the silicate band (Fig. 1). Both HH 46 IRS and B5 IRS 1 show prominent bands of solid CO at 4.67 μm (Fig. 2*d*). The ratio between the central narrow CO component and the broad long-wavelength wing, representing the column density ratio of volatile pure CO and CO mixed with less volatile H_2O, is a factor of 5 smaller in HH 46 IRS. In fact, the profile of HH 46 IRS is comparable to that of the massive protostar W33A. The
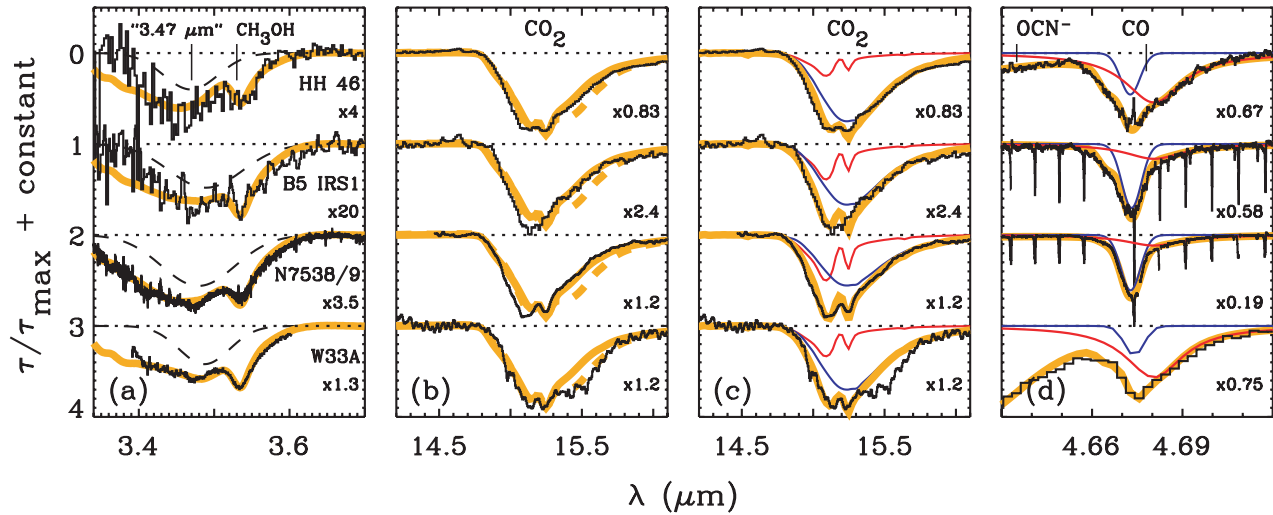
Fig. 2.—Solid CH_3OH, CO_2, and CO spectra of HH 46 IRS and B5 IRS 1 compared with the massive protostars NGC 7538 IRS 9 and W33A in each panel (*top to bottom*). The normalization factor is indicated in the right corner of each plot. (*a*) A laboratory pure CH_3OH spectrum at $T_{lab} = 10$ K (*thick yellow line*) to which is added a Gaussian (*dashed line*) to account for the underlying "3.47 μm" absorption feature. The NGC 7538 IRS 9 and W33A data are from Boogert et al. (2004) and Brooke et al. (1999), respectively. (*b*) The CO_2 bending mode observed with *Spitzer* IRS (HH 46 IRS and B5 IRS 1) and *ISO* SWS (NGC 7538 IRS 9 and W33A). The thick yellow dashed line is the laboratory ice $H_2O:CH_3OH:CO_2 = 0.84:0.92:1$, and the solid thick, yellow line is a laboratory ice with reduced CH_3OH content, $H_2O:CH_3OH:CO_2 = 0.92:0.29:1$, both at $T_{lab} = 115$ K. Only for W33A is an enhanced $CH_3OH:CO_2$ ratio required, in agreement with the strong 3.53 μm CH_3OH feature in (*a*). (*c*) The CO_2 bending mode for the same sources as in (*b*), but now fitted with different laboratory spectra: a highly processed polar ice ($T_{lab} = 125$ K; *red line*) in combination with an H_2O-rich, CH_3OH-deficient cold ice ($T_{lab} = 10$ K; *blue line*). The sum of these two components is the thick yellow line. (*d*) The absorption band of solid CO observed with VLT ISAAC (HH 46 IRS), Keck NIRSPEC (B5 IRS 1 and NGC 7538 IRS 9), and *ISO* SWS (W33A). Narrow absorption lines are due to circumstellar gas-phase CO. The onset of the 4.62 μm "XCN" band is seen in HH 46 IRS and W33A. Gaussian and Lorentzian fits to the apolar and polar CO components are indicated by blue and red lines (Pontoppidan et al. 2003b). The thick yellow line represents the combined fit, including the XCN band and a blueshifted CO component, which are not shown separately.

latter two sources also show a band at 4.62 μm, most likely attributed to the OCN^- ion. Relative to H_2O, the OCN^- column density is comparable to (upper limits to) those of B5 IRS 1 and NGC 7538 IRS 9. Furthermore, the 4.67 μm spectrum of B5 IRS 1 shows deep rovibrational gas-phase CO lines. The presence of gas-phase CO in HH 46 IRS is hard to assess because of telluric contamination. The intriguing differences and similarities between HH 46 IRS and B5 IRS 1, as well as compared to massive protostars, provide insight into the formation and evolution of interstellar and circumprotostellar ices.

Finally, column densities of the main ices, summarized in Table 1, are derived by dividing the integrated optical depth over the laboratory integrated band strength (e.g., Hudgins et al.

1993). Note that the $CO_2:H_2O$ ratios toward B5 IRS 1 and HH 46 IRS are significantly larger than the average over many, mostly massive protostellar sight lines (0.17 ± 0.03; Gerakines et al. 1999).

4. DISCUSSION

4.1. *Evolution of Ices in Low-Mass Environments*

The formation and evolution of interstellar ices is, in principle, strongly dependent on local conditions such as the atomic hydrogen and carbon density, the temperature, the cosmic-ray flux, the ultraviolet photon flux, and the presence of shocks. Thus, key issues are the location of the ices along the absorption line of sight and the relative contributions from foreground clouds, envelopes, and inclined disks. The continuous rise of both the B5 IRS 1 and HH 46 IRS spectral energy distributions (SEDs) between 3 and 40 μm, as well as the detection of extended submillimeter emission in James Clerk Maxwell Telescope archive images, are in favor of envelope-dominated models. We established the properties of these envelopes using the approach of Jørgensen et al. (2002). Adopting optical constants for bare and ice-coated silicate grains (Ossenkopf & Henning 1994), the 2–2000 μm SED and the depth of the observed superposed ice and silicate bands were self-consistently modeled. The SED and silicate band depth of B5 IRS 1 are well fitted by the envelope models, and a significant fraction of the ices has evaporated. In contrast to B5 IRS 1, the submillimeter/far-infrared and mid-infrared *Spitzer* SED of HH 46 IRS cannot be simultaneously fitted. Possibly, this envelope is embedded in a larger scale, cold cloud not modeled within the framework of the simple spherical envelope.

Next we address the extent to which the ices in these envelopes have been processed. Several indicators are available. Laboratory experiments have shown that heating of ice

TABLE 1
Column Densities and Abundances

Quantity	B5 IRS 1	HH 46	N7538/9[a]	W33A[b]
$N(CO_2)/N(H_2O)$..............	0.37	0.32	0.24	0.16
$N(CO\text{-}p)/N(H_2O)$[c]...........	0.16	0.15	0.02	0.08
$N(CO\text{-}np)/N(H_2O)$[d]........	0.27	0.05	0.14	0.03
$N(CH_3OH)/N(H_2O)$........	<0.06	0.07	0.07	0.22
$N(OCN^-)/N(H_2O)$[e].........	<0.005	0.007	0.006	0.02
$N(H_2O)$ (10^{18} cm^{-2})	2.2 (0.3)	8.0	6.8	9.0
$N(H_2O)/N_H$ (10^{-5})..........	5.2	5.7	5.0	3.2
N_H (10^{22} cm^{-2})	4[f]	14[f]	16	28

[a] Whittet et al. (1996) and references therein.
[b] Gibb et al. (2000) and references therein.
[c] Broad "polar" CO component, likely H_2O mixture.
[d] Broad "apolar" CO component, likely pure CO.
[e] Using OCN^- band strength of van Broekhuizen et al. (2004).
[f] From the envelope models described in the text.

mixtures with concentrations of $CO_2/H_2O \geq 1$ results in crystallization and an effective segregation of the CO_2 and H_2O species. Spectroscopically, this is recognized as a double-peaked profile, characteristic of the pure CO_2 matrix (Ehrenfreund et al. 1998). Depending on the ice composition, the amorphous-to-crystalline phase transition occurs at 50–90 K in space, lower than the corresponding laboratory temperatures owing to the longer interstellar timescales (Boogert et al. 2000). Sub-structures are seen in the HH 46 IRS CO_2 band (Fig. 2b), but they are much weaker than some highly heated massive protostellar envelopes (Gerakines et al. 1999) and are absent in B5 IRS 1. In fact, the CO_2 band profile of HH 46 IRS is comparable to that observed toward one of the least processed envelopes, sur-rounding the massive protostar NGC 7538 IRS 9. In the simplest scenario of a single ice at one temperature, the mixture $CH_3OH:H_2O:CO_2 = 0.3:1:1$ (§ 4.2) must still have a lab-oratory temperature as high as 115 K, or ∼75 K in space (Fig. 2b). In the more likely scenario of a temperature gradient along the line of sight, the bulk of the HH 46 IRS and B5 IRS 1 envelopes have temperatures well below 50 K. A fraction of the inner envelope of HH 46 IRS must be warmer, causing the ob-served weak substructures. Such two-component fits explain the observed profiles well (Fig. 2c).

More extensive processing at lower temperatures most likely has occurred within the envelopes, however. Unlike the mas-sive protostar NGC 7538 IRS 9, the ground-based 4.67 μm spectra of solid CO toward HH 46 IRS and B5 IRS 1 show a weak central narrow component (Fig. 2d; Table 1). The most volatile CO-rich "apolar" ices may thus have evaporated (Tielens et al. 1991). HH 46 IRS shows a particularly broad profile, resembling the massive protostar W33A. Like W33A, HH 46 IRS shows an absorption feature at 4.62 μm, likely attributed to the OCN$^-$ species. This molecule may be produced from HNCO in the solid state at relatively low ice temperatures of less than 50 K (van Broekhuizen et al. 2004).

Concluding, while high-temperature ice processing, traced by the CO_2 band, is not observed in the low-mass envelopes, low-temperature (<50 K) processing may play a significant role. Qualitatively this is similar to some high-mass protostars (W33 A, NGC 7538 IRS 9). The proposed evolutionary se-quence of ice processing in massive envelopes (Boogert et al. 2000; van der Tak et al. 2000) is indeed largely based on high-temperature indicators, such as ice crystallization, hot core gas temperatures, and gas/solid state ratios. These relations need to be investigated in a larger sample of low-mass protostars, in which the CO_2 band profile is a crucial tracer.

4.2. $CH_3OH:CO_2$ *Complexes*

The long-wavelength wing of the CO_2 bending mode may be a tracer of the presence of CH_3OH in the ices. CO_2 and CH_3OH form complexes, leading to an enhanced wing in some sources well fitted by laboratory ices with a $CH_3OH:H_2O:CO_2$ mix-ing ratio of 1:1:1 (e.g., W33A in Fig. 2b). Recently, large abundances of CH_3OH of 25% with respect to H_2O were found in the envelopes of some low-mass protostars (Pontoppidan et al. 2003a). Clearly, B5 IRS 1 and HH 46 IRS both have lower CH_3OH abundances (Table 1). This is consistent with the weakness of the long-wavelength CO_2 wing. Indeed, lab-oratory mixtures with a $CH_3OH:H_2O:CO_2$ ratio of 0.3:1:1 fit the observed band well. The high $CO_2:CH_3OH$ column den-sity ratio of ∼6 toward these sources is, however, barely consistent with this laboratory mixture. Alternatively, the band profile can be explained by the combination of an abundant H_2O-rich ice responsible for the long-wavelength wing and an at least partly heated CO_2-rich ice responsible for the crystal-lization substructures seen in HH 46 IRS (Fig. 2c).

5. CONCLUSIONS AND FUTURE WORK

High-quality *Spitzer* observations of the CO_2 bending mode at 15 μm toward low-mass protostars offer a new tracer of ice mantle composition and evolution. The embedded low-mass systems B5 IRS 1 and HH 46 IRS show CH_3OH-poor ices with little evidence for 50–90 K thermal processing in their enve-lopes. Lower temperature processing appears evident in the solid CO band. These results form the basis for future studies on the physical and chemical state of ices entering proto-planetary disks and on how these and solar system ices are related. CO_2 bending-mode observations of more evolved systems and edge-on disks are required.

REFERENCES

Beichman, C. A., et al. 1984, ApJ, 278, L45
Boogert, A. C. A., Blake, G. A., & Öberg, K. 2004, ApJ, submitted
Boogert, A. C. A., et al. 2000, A&A, 353, 349
Brooke, T. Y., Sellgren, K., & Geballe, T. R. 1999, ApJ, 517, 883
Charnley, S. B., Whittet, D. C. B., & Williams, D. A. 1990, MNRAS, 245, 161
Chiar, J. E., et al. 2000, ApJ, 537, 749
Ehrenfreund, P., Dartois, E., Demyk, K., & D'Hendecourt, L. 1998, A&A, 339, L17
Evans, N. J., et al. 2003, PASP, 115, 965
Gerakines, P. A., et al. 1999, ApJ, 522, 357
Gibb, E. L., et al. 2000, ApJ, 536, 347
Houck, J. R., et al. 2004, ApJS, 154, 18
Hudgins, D. M., Sandford, S. A., Allamandola, L. J., & Tielens, A. G. G. M. 1993, ApJS, 86, 713
Jørgensen, J. K., Schöier, F. L., & van Dishoeck, E. F. 2002, A&A, 389, 908
Kessler-Silacci, J. E., Hillenbrand, L. A., Blake, G. A., & Meyer, M. R. 2004, ApJ, submitted

Langer, W. D., Velusamy, T., & Xie, T. 1996, ApJ, 468, L41
McLean, I. S., Becklin, E. E., Bendiksen, O., Brims, G., & Canfield, J. 1998, Proc. SPIE, 3354, 566
Moorwood, A., et al. 1999, Messenger, 95, 1
Noriega-Crespo, A., et al. 2004, ApJS, 154, 352
Ossenkopf, V., & Henning, T., 1994, A&A, 291, 943
Pontoppidan, K. M., Dartois, E., van Dishoeck, E. F., Thi, W.-F., & d'Hendecourt, L. 2003a, A&A, 404, L17
Pontoppidan, K. M., et al. 2003b, A&A, 408, 981
Tielens, A. G. G. M., Tokunaga, A. T., Geballe, T. R., & Baas, F. 1991, ApJ, 381, 181
van Broekhuizen, F. A., Keane, J. V., & Schutte, W. A. 2004, A&A, 415, 425
van der Tak, F. F. S., van Dishoeck, E. F., Evans, N. J., & Blake, G. A. 2000, ApJ, 537, 283
Werner, M. W., et al. 2004, ApJS, 154, 1
Whittet, D. C. B., et al. 1996, A&A, 315, L357